NJC

ROYAL SOCIETY OF CHEMISTRY

PAPER

Check for updates

Cite this: *New J. Chem.*, 2022, **46**, 12342

Mixed-ligand copper(II) complexes of guanidine derivatives containing ciprofloxacin: synthesis, characterization, DFT calculations, DNA interactions and biological activities†

Prangtip Nonkuntod,[a] Atittaya Meenongwa,[b] Thanaset Senawong,[c] Chaiyaporn Soikum,[d] Prapansak Chaveerach,[d] Athis Watwiangkham,[e] Suwit Suthirakun[e] and Unchulee Chaveerach*[a]

Two mixed-ligand complexes of copper(II) chloride containing guanidine derivatives and ciprofloxacin (HCip), namely [CuL^{1m}(Cip)]Cl (**1Cip**) and [CuL^{2m}(Cip)]Cl (**2Cip**) (L^{1m} = amidino-*O*-methylurea, L^{2m} = *N*-(benzyl)-amidino-*O*-methylurea), were synthesized and characterized by elemental analysis and spectroscopic techniques, including density functional theory (DFT) calculations. The possible coordination geometry of **1Cip** and **2Cip** was predicted to be distorted square planar. The binding mode and strength of the complexes to calf thymus (CT) DNA were explored using absorption titration, viscosity measurements, circular dichroism and fluorescence spectroscopies, which suggested intercalation between the DNA-bases as the most probable binding mode. The intrinsic binding constants (K_b) were determined and found in the trend of **2Cip** > **1Cip**. Analysis of the cleaving ability of the complexes toward pBR322 plasmid DNA in the absence and presence of hydrogen peroxide was also carried out by gel electrophoresis. The results of our studies suggest that the main cleaving pathway of **1Cip** and **2Cip** may occur *via* an oxidative mechanism. Their cytotoxicity was then tested against human cervical cancer (HeLa) and breast cancer (MCF-7) cells in comparison to normal kidney (Vero) cells. The studied complexes showed greater anticancer activity against both cancer cells than HCip and the starting compounds (**1** and **2**). In addition, the complexes are inactive toward normal cells, probably due to their additional ciprofloxacin. The mechanism of cell death was further investigated by flow cytometry, and it was found that **1Cip** and **2Cip** may induce the death of the cancer cells *via* apoptosis pathways in the S phase for HeLa cells, and the G0/G1 phase for MCF-7 cells. The antibacterial activities of the complexes were also tested against three human food poisoning bacteria (*E. coli*, *Salmonella*, and *Campylobacter*). According to the MIC values, the antibacterial activity of **1Cip** and **2Cip** was the best against *Salmonella* (1.95 μg mL^{-1}).

Received 21st March 2022,
Accepted 27th May 2022

DOI: 10.1039/d2nj01377k

rsc.li/njc

1. Introduction

Following the discovery of the anticancer activity of cisplatin (*cis*-[Pt(NH$_3$)$_2$Cl$_2$]) in 1965,[1] the metal complexes used as anticancer agents have mostly comprised Pt(II) compounds, which exhibit several side effects due to the lack of selectivity. Many research groups have been interested in these drawbacks and have attempted to identify new metal complexes possessing high therapeutic properties, but with fewer or no side effects. Complexes with transition metals such as Co(II), Cu(II), Zn(II), Au(I), Au(III), Fe(II), Ni(II), Pd(II) and Ru(II) have been synthesized, and their cytotoxicity toward cancer cells has been investigated.[2–4] In the current study, copper was selected since it is an essential trace element in the body that exhibits low toxicity and plays an important role in the immune system and nerve cells.[5]

[a] *Materials Chemistry Research Centre, Department of Chemistry and Centre of Excellence for Innovation in Chemistry, Faculty of Science, Khon Kaen University, Khon Kaen 40002, Thailand. E-mail: sunchul@kku.ac.th*
[b] *Health Science and Aesthetic Program, Department of Science, Faculty of Science and Technology, Rajamangala University of Technology Krungthep, Bangkok 10120, Thailand*
[c] *Department of Biochemistry, Faculty of Science, Khon Kaen University, Khon Kaen 40002, Thailand*
[d] *Department of Veterinary Public Health, Faculty of Veterinary Medicine, Khon Kaen University, Khon Kaen 40002, Thailand*
[e] *School of Chemistry, Institute of Science, Suranaree University of Technology, Nakhon Ratchasima 30000, Thailand*

† Electronic supplementary information (ESI) available. See DOI: https://doi.org/10.1039/d2nj01377k

 This journal is © The Royal Society of Chemistry and the Centre National de la Recherche Scientifique 2022

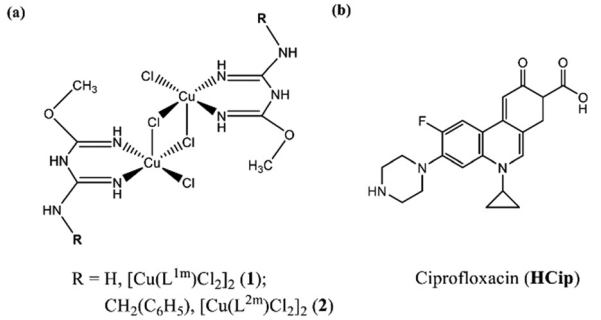

Fig. 1 (a) The starting compounds and (b) ciprofloxacin.

Copper complexes with diverse organic ligands also exhibit a wide spectrum of biological properties such as antibacterial,[6] antifungal,[7] anti-inflammatory[8] and antiviral activities.[9] Thus, copper-based complexes are among the best choices for cancer therapy. *N*,*N*-Bidentate amidino-*O*-alkylurea and its derivatives comprise one of the most interesting ligand systems because they possess many hydrogen-bonding groups and are very stable after coordination with copper ions. In 2015, the copper(II) complexes containing 1-amidino-*O*-methylurea (L^{1m}) and *N*-(benzyl)-amidino-*O*-methylurea (L^{2m}), namely $[Cu(L^{1m})Cl_2]_2$ (**1**) and $[Cu(L^{2m})Cl_2]_2$ (**2**), which adopt a square-pyramidal geometry, were synthesized and their anticancer activities were studied and reported on by our research groups (Fig. 1(a)).[10] Complexes **1** and **2** have shown DNA cleavage and DNA-binding abilities through non-intercalative modes. Their anticancer activities against lung cancer (NCl-H187) have been reported with IC_{50} values of 49.42 μg mL^{-1} for **1** and 47.63 μg mL^{-1} for **2**.[10] In an attempt to enhance the anticancer potential, the interactions of **1** and **2** with another ligand which is, in this work, ciprofloxacin, should be considered of great importance and further evaluated.

Ciprofloxacin (HCip) (Fig. 1(b)) is an antibacterial drug used to treat diverse infections caused by Gram-negative bacteria, such as urinary tract infections, lower respiratory tract infections, bone and joint infections, and typhoid fever.[11] In addition, ciprofloxacin can act as an *O*,*O*-bidentate ligand and coordinate with transition metals through a pyridone oxygen and one carboxylate oxygen. According to the literature, several metal complexes of HCip in the deprotonated form, including Mn(II), Fe(III), Co(II), Ni(II), Mo(II) and Cu(II),[12,13] have been studied in an attempt to investigate the structure, spectroscopic and biological properties, such as antituberculosis,[14] antibacterial,[15] antimicrobial,[16] anticancer[17] and antifungal[18] attributes. The mechanism of biological action of HCip is believed to inhibit DNA gyrase, an essential bacterial enzyme that maintains superhelical twists in DNA.[19]

In order to improve the biological activity of copper(II) complexes, in the present work, we have synthesized, characterized, and studied the cytotoxicity of two new mixed-ligand copper(II) complexes containing 1-amidino-*O*-methylurea (L^{1m}) or *N*-(benzyl)-amidino-*O*-methylurea (L^{2m}) and ciprofloxacin, $[CuL^{1m}(Cip)]Cl$ (**1Cip**) and $[CuL^{2m}(Cip)]Cl$ (**2Cip**), respectively. These two complexes are characterized by infrared, diffuse reflectance, UV-Visible, mass and electron paramagnetic resonance spectroscopies and DFT calculations. A major aim is to investigate the potential anticancer activities of the complexes containing ciprofloxacin compared to the relevant starting compounds (**1** and **2**). The binding property of the complexes towards calf thymus (CT) DNA was examined by the absorption titration method, circular dichroism (CD) spectroscopy, competitive binding study using fluorescence spectroscopy, and viscosity measurements. Additionally, the cleaving ability of the complexes toward plasmid pBR322 DNA was evaluated by gel electrophoresis. Data on the biological activities of the synthesized complexes acting as a drug were investigated by using the MTT assay. An apoptosis assay and cell cycle arrest were used to investigate the mechanism of cell death caused by the complexes. Finally, antibacterial activity was investigated by the agar-well diffusion method.

2. Experimental

2.1 Materials and physical measurements

Copper(II) chloride dihydrate ($CuCl_2{\cdot}2H_2O$), hydrochloric acid 37% (HCl), *n*-butanol 99%, methanol (MeOH), dimethyl sulfoxide (DMSO), sodium hydroxide (NaOH), benzylamine, ethidium bromide (EB), *cis*-diammineplatinum(II) dichloride (cisplatin), and sodium salt of calf thymus DNA (CT-DNA, type I fibrous) were purchased from Sigma-Aldrich. Sodium dicyanamide 97%, and ciprofloxacin 98% (HCip) were purchased from Acros organics. Plasmid pBR322 DNA and Tris hydrochloric acid (Tris–HCl) were obtained from Bio Basic INC. All chemical reagents were used as received without further purification.

Melting points were measured on Electrothermal IA9000 Series melting point apparatus. FT-IR spectra (4000–600 cm^{-1}) were recorded on a Bruker TENSOR27 ATR-FTIR spectrophotometer. Elemental analyses (C, H and N) were performed with a PerkinElmer PE 2400 CHNS analyzer. Electrospray ionization mass spectra (ESI-MS) in positive mode were obtained on a liquid chromatography-micrOTOF-benchtop ESI-TOF-MS spectrometer. Electronic absorption spectra were recorded on an UV-Vis spectrophotometer, Agilen8453 (for solution phase), using quart cuvettes of 1 cm path length, and an UV-Vis-NIR scanning spectrophotometer, Shimadzu 3101 (for solid phase). Electron paramagnetic resonance (EPR) spectra were detected by a Bruker EMXmicro spectrometer at 9.40 GHz frequency (X-band). Circular dichroism (CD) spectra using a 1 cm quartz cuvette were recorded on a Jasco J-815 spectropolarimeter. Fluorescence spectra were acquired on a FS5 Spectrofluorometer. Cell growth inhibition was collected by a Bio-Rad 680 microplate reader. The mechanism of cell death was investigated using a BD FACSCalibur flow cytometer.

2.2 Synthesis of the copper(II) complexes of guanidine derivatives

The blue copper(II) complexes $[CuL^{1m}Cl_2]_2$ (**1**) and $[CuL^{2m}Cl_2]_2$ (**2**) were used as a starting compound and synthesized according to the procedures reported in our previous work.[20]

2.3 Synthesis of the mixed-ligand complexes (1Cip and 2Cip)

The starting compounds **1** (0.0501 g, 0.2 mmol) for **1Cip** or **2** (0.0681 g, 0.2 mmol) for **2Cip** in methanol (20 mL) were added to ciprofloxacin (HCip) (0.1325 g, 0.4 mmol) deprotonated by 1 M NaOH (0.4 mL, 0.4 mmol). The resulting mixtures were stirred at ambient temperature for 2 h for **1Cip** and 4 h for **2Cip**. The purple products were obtained, filtered off and dried in a vacuum desiccator.

[CuL^{1m}(Cip)]Cl (**1Cip**). Purple solid, yield: 72.3% (0.0788 g, 0.14 mmol). m.p. (°C): 215.0–217.5. Anal. calc. for $C_{20}H_{25}N_7O_4F$-CuCl (M_W = 545.42): C, 44.04; H, 4.62; N, 17.98%; found: C, 43.91; H, 4.54; N, 17.10%. IR (cm^{-1}): 3358br, 2951w, 2838m, 1613s, 1577s, 1513w, 1476s–1457s, 1376s, 1302m, 1254s, 1196w–1112w, 1043w–1027m, 946s, 896w–701m, 655m–629m. Diffuse reflectance (λ/nm, cm^{-1}): 562.0, 17 794. UV-Vis (2 mM in hot MeOH) (λ/nm, cm^{-1}): 572.0, 17 483. MS (ESI positive ion), *m*/*z*: 332, $[HCip+H]^+$; 509, $[CuL^{1m}(Cip)]^+$.

[CuL^{2m}(Cip)]Cl (**2Cip**). Purple solid, yield: 79.2% (0.1006 g, 0.16 mmol). m.p. (°C): 235.0–238.0. Anal. calc. for $C_{27}H_{31}N_7O_4F$-CuCl (M_W = 635.53): C, 51.02; H, 4.92; N, 15.43%; found: C, 51.12; H, 5.46; N, 15.26%. IR (cm^{-1}): 3238br, 2947w, 2836w, 1613s, 1579s, 1523s, 1479m, 1459m, 1374m, 1352w, 1335w, 1259s, 1192m–1095w, 1050m, 1019w, 946m, 898w. Diffuse reflectance (λ/nm, cm^{-1}): 556.0, 17 986. UV-Vis (2 mM in hot MeOH) (λ/nm, cm^{-1}): 578.0, 17 301. MS (ESI positive ion), *m*/*z*: 332, $[HCip+H]^+$; 599, $[CuL^{2m}(Cip)-H]^{2+}$.

2.4 Density functional theory (DFT) calculations

All calculations were carried out using the Turbomole package.[21,22] Gas-phase geometries of the studied compounds were optimized at the ground state using the hybrid functional B3LYP[23,24] with the def2-TZVP basis set.[25] The optimized geometries were visualized using the VESTA program.[26]

To determine the relative stabilities of **1Cip** and **2Cip** in different configurations, their binding energies (E_b) were calculated from eqn (1).

$$E_b = E_C - E_M - \Sigma E_L \quad (1)$$

where E_C, E_M, and E_L are the energies of the metal–ligand complex, metal atom, and ligands, respectively. The more negative the binding energies are, the higher the stability of the complexes is.

2.5 Stability determination

The stability of **1Cip** and **2Cip** in Tris-buffer containing 0.3% DMSO was monitored at seven different time points (0, 3, 6, 12, 24, 48 and 72 h) by UV-Vis spectrophotometry at room temperature. Rate constants (k) and half-lives ($t_{1/2}$) were calculated by fitting the concentration of the complex, ln(c), calculated from the UV-Visible absorbance changes to the pseudo first-order kinetics equation. The concentration values at different time points (0–72 h) were plotted and k is given by the slope of the linear fit, while $t_{1/2} = \ln(2)/k$.[27]

2.6 DNA binding studies

The stock DNA solution was performed using calf thymus (CT) DNA in Tris-buffer (containing 5 mM Tris–HCl and 50 mM NaCl at pH 7.1). The concentration of CT-DNA was determined by UV absorbance at 260 nm with the molar absorption coefficient value of 6600 M^{-1} cm^{-1}.[28] The absorbance spectra of CT-DNA solution give a ratio of the bands at 260 nm and 280 nm with a 1.8 : 1 ratio, suggesting that the CT-DNA is protein-free.[29] The DNA stock solution was kept in 4 °C and used within 4 days. In addition, the complex stock solutions of **1Cip** and **2Cip** were dissolved in Tris-buffer containing 0.3% DMSO for all experiments. All stock solutions were freshly prepared before use.

2.6.1 Absorption titration experiments. Absorption spectra of the mixed-ligand complexes (**1Cip** and **2Cip**) were performed by using different concentrations of CT-DNA (0, 20, 40, 60, 80, and 100 μM), and a constant concentration of **1Cip** and **2Cip** (50 μM) in Tris-buffer containing 0.3% DMSO at 37 °C for 24 h. The spectra were recorded using a UV-Vis spectrophotometer at room temperature. To subtract the absorption due to the DNA itself (in each sample), the reference solutions (free CT-DNA) at the corresponding concentrations (0–100 μM) were used before recording the absorption band of each sample. This technique can determine the binding affinity between CT-DNA and the complexes by calculating the intrinsic binding constant (K_b), using the Wolfe–Shimer eqn (2).[30]

$$[DNA]/(\varepsilon_a - \varepsilon_f) = [DNA]/(\varepsilon_b - \varepsilon_f) + 1/K_b(\varepsilon_b - \varepsilon_f) \quad (2)$$

where [DNA] is the concentration of DNA, ε_a is given by A_{obs}/[Cu], and ε_f and ε_b are free and fully bound compounds, respectively. K_b is given by the ratio of the slope to the y intercept.

2.6.2 Viscosity measurements. Viscosity measurements were performed using an Ubbelodhe viscometer in a water bath at a constant temperature of 37.0 ± 0.1 °C. The concentration of CT-DNA was kept constant (50 μM) with varying the [Complex]/[DNA] ratios in the range of 0.00–2.00 with 0.20 intervals in Tris-buffer containing 0.3% DMSO. Flow times for each sample were recorded three times, using a digital stopwatch and the average flow time was calculated. Relative viscosity values (η) were calculated from $\eta = (t - t_0)/t_0$, where t is the observed flow time of DNA containing the complexes at various concentrations and t_0 is the flow time of Tris-buffer alone.[31] The data are presented as $(\eta/\eta_0)^{1/3}$ *vs.* [Complex]/[DNA] ratios, where η_0 and η are the viscosity of the free DNA solution and the DNA–complex solution, respectively.

2.6.3 Circular dichroism spectroscopy. The solution of CT-DNA was kept constant (50 μM) in the presence of the **1Cip** and **2Cip** (0, 25 and 50 μM) in Tris-buffer containing 0.3% DMSO at 37 °C for 24 h. The CD spectra of these solutions were recorded from 200 to 400 nm using a quartz cuvette with an optical path length of 1 mm and a scanning rate of 50 nm min^{-1}. The data were collected in triplicate with a time constant of 1 s and a spectral bandwidth of 1.0 nm.

2.6.4 Fluorescence titration experiments. The different concentrations of the complexes (0, 20, 40, 60, 80, and 100 μM)

 This journal is © The Royal Society of Chemistry and the Centre National de la Recherche Scientifique 2022

in Tris-buffer containing 0.3% DMSO were added into the EB–DNA solution (50 μM EB and 50 μM CT-DNA). These mixture solutions were kept in the dark for 30 min before measurement. The excitation wavelength was 510 nm and the emission data were recorded from 530 to 800 nm. The possible fluorescence quenching mechanism can be interpreted using the classical Stern–Volmer eqn (3).[32]

$$F_0/F = 1 + K_{SV}[Q] \quad (3)$$

where F_0 and F are the fluorescence intensities of the EB–DNA in the absence and presence of the metal complex [Q], respectively. K_{SV} is the Stern–Volmer quenching constant, which can be obtained as the slope of F_0/F *versus* [Q]. Furthermore, the apparent binding constant (K_{app}) was utilized to determine the strength of the binding between the complexes and DNA using eqn (4).[33]

$$K_{EB}[EB] = K_{app}[Complex] \quad (4)$$

where [Complex] is the concentration of the complex at a 50% reduction of the fluorescence intensity of EB and K_{EB} is 1.0×10^7 M^{-1} ([EB] is 50 μM).

2.7 DNA cleavage studies

Nuclease activity of the complexes was investigated by agarose gel electrophoresis. Tris-buffer containing 0.3% DMSO was used as a solvent. The samples were prepared by mixing plasmid pBR322 DNA (0.2 μg) with the complexes (10, 50, 100, 200, 300, 400, 500 and 1000 μM) in Tris-buffer containing 0.3% DMSO (10 μL) and incubated at 37 °C for 4 h. A loading dye (2 μL) was added into the samples after incubation and subjected into 0.8% agarose gel immersed in a 1X TAE running buffer at 50 V for 1.5 h. After electrophoresis, the gel was stained with EB for 5 min and photographed under UV light. To explore the possible DNA cleavage mechanism, H_2O_2 (10 μM) as a reducing agent was further added into the samples containing plasmid pBR322 DNA and the complexes, and then incubated at 37 °C for 1 h. The efficiency of DNA cleavage can be determined by the %DNA cleavage activity, which is calculated from eqn (5).[34]

$$\%\text{DNA cleavage activity} = \{[(\text{Volume of DNA Form I})_{\text{control}} - (\text{Volume of DNA Form I})_{\text{sample}}]/(\text{Volume of DNA Form I})_{\text{control}}\} \times 100 \quad (5)$$

where the volume is band intensity × area of supercoiled DNA (Form I).

2.8 Cell culture

The cytotoxicity effects of **1Cip** and **2Cip** against two human cancer cell lines, cervical (HeLa) and breast carcinoma (MCF-7), and a normal kidney (Vero) cell line were investigated using the MTT (3-(4,5-dimethylthiazol-2-yl)-2,5-diphenyltetrazolium bromide) assay. All cells were maintained in RPMI1640 medium with 10% fetal bovine serum (FBS), penicillin (100 U mL^{-1}), and streptomycin (100 μg mL^{-1}) (Gibco-BRL, USA) in a humidified atmosphere containing 5% CO_2 at 37 °C. Tris-buffer containing 0.3% DMSO was used as a solvent control. Cisplatin was used as a positive control for all cytotoxicity experiments.

2.8.1 MTT assay. Cells were seeded in 96-well microplates (8×10^3 cells per well) at 37 °C. After 24 h, the cells were treated with different concentrations of the complexes (0, 10, 20, 40, 60, 80, and 100 μg mL^{-1}) and incubated at 37 °C for 24, 48 and 72 h. Then, the MTT solution (0.5 μg mL^{-1}) was added to each well and kept at 37 °C for 3 h. Subsequently, the solution was removed and 100 μL of DMSO was added to solubilize the formazan crystals at 37 °C for 10 min. The absorbance of formazan was measured by using a microplate reader at 550 nm (A_{550}) with a reference wavelength of 655 nm (A_{655}) to remove the background. The anticancer activity of the copper(II) complexes was expressed as 50% inhibitory concentration (IC_{50}) and calculated using eqn (6).[35]

$$\%\text{ Cell viability} = [\text{Sample}_{(A_{550} - A_{655})}/\text{Control}_{(A_{550} - A_{655})}] \times 100 \quad (6)$$

The complexes with $IC_{50} > 50$ μg mL^{-1} were considered to be inactive.

2.8.2 Apoptosis assay. HeLa and MCF-7 cells were seeded in cell plates at a density of 1×10^6 cells per well and incubated at 37 °C for 24 h. After 24 h incubation, cells were treated with 50 μg mL^{-1} of the complexes compared to the positive control cisplatin (25 μg mL^{-1}). Tris-buffer containing 0.3% DMSO was used as a solvent control. After 48 h, the cells were washed, collected and resuspended in 100 μL Annexin-binding buffer. Then, the cells were stained with 5 μL Annexin V-FITC and 2 μL of propidium iodide (PI) for 15 min at room temperature in the dark. Finally, the samples were measured using a flow cytometer. The dot plots of the induction of apoptosis by using PI and FITC-Annexin V assay show percentage of living cells (Annexin V FITC−/PI−, Q1), early apoptotic cells (Annexin V FITC+/PI−,Q2), late apoptotic cells (Annexin V FITC+/PI+, Q3), and necrotic cells (Annexin V FITC−/PI+, Q4).

2.8.3 Cell cycle analysis. HeLa and MCF-7 cells were seeded in a 60 × 15 mm dish at a density of 1×10^6 cells per plate and incubated at 37 °C for 24 h. Each plate was treated with 50 μg mL^{-1} of the complexes and incubated at 37 °C. After 48 h, the cells were harvested and washed twice with ice-cold phosphate buffered saline (PBS). The cells were permeabilized in 70% cold EtOH at 4 °C for 1 h, washed with PBS, added with 5 μL of RNase (20 mg mL^{-1}) and incubated at room temperature for 30–45 min. Finally, the cells were stained with 5 μL of PI for 30 min and analyzed by flow cytometry.

2.8.4 Antibacterial activity. Antibacterial activities of the complexes against three Gram-negative bacteria, namely *E. coli*, *Salmonella* and *Campylobacter* (1×10^8 CFU mL^{-1}) were performed by the agar-well diffusion method.[36] Each bacteria was transferred into 0.75% (w/w) semisolid Brucella agar (10 mL) at 50 °C. Then, the incubated medium was swirled to distribute the cell culture of bacteria and held at room temperature for 30 min. Wells were prepared in the agar plates using a sterile cork of 6.0 mm diameter. The plates were placed at 37 °C for 48 h under the appropriate conditions to allow cell culture growth. The stock solution of all complexes (250 μg mL^{-1}) was

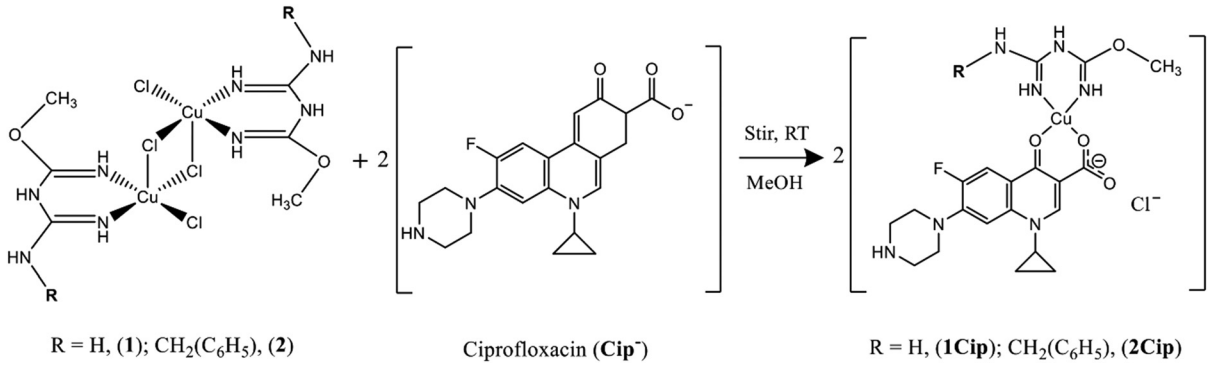

Scheme 1 Synthetic routes of **1Cip** and **2Cip**.

dissolved in Tris-buffer containing 0.3% DMSO and then transferred into a well aseptically. The minimum inhibitory concentration (MIC) values were also determined by the two-fold serial dilution method.[37] The experiments were carried out in triplicate. Ciprofloxacin was use as a positive control.

2.9 Statistical analysis

All data in the parts of the DNA interactions and biological activity were collected in three separate experiments. The statistical program SPSS version 17.0 for windows (SPSS Corporation, Chicago, IL) was used to conduct the analyses. The criterion for the significant difference was set at $^{*}P < 0.01$.

3. Results and discussion

3.1 Synthesis and characterization of the complexes

The mixed-ligand complexes (**1Cip** and **2Cip**) were successfully synthesized in relatively high yield (72–80%) by the reaction of the appropriate starting compounds $[CuL^{1m}Cl_2]_2$ (**1**) or $[CuL^{2m}Cl_2]_2$ (**2**) with ciprofloxacin in a 1 : 2 molar ratio (Scheme 1). The change in color from blue (for **1** and **2**) to purple (for **1Cip** and **2Cip**) was observed when the reactions were complete, indicating that the environment around the copper(II) center had been altered. Both **1Cip** and **2Cip** are stable in air and easily soluble in DMSO, but dissolve only partially in hot methanol and water. Results from the elemental analysis of the mixed-ligand complexes are in good agreement with theoretical expectations. Their proposed structures are shown in Scheme 1. Further characterization of the complexes was undertaken by infrared, mass, electron paramagnetic resonance and UV-Visible spectroscopic techniques.

FT-IR spectra of the starting compounds (**1** and **2**), the mixed-ligand complexes (**1Cip** and **2Cip**), and ciprofloxacin (HCip) were recorded, as shown in Fig. 2. The characteristic absorption bands corresponding to the functional groups from the starting compounds and HCip ligand were found in the infrared spectra of **1Cip** and **2Cip** (Table S1, ESI†). Broad bands in the region of 3400–3100 cm^{-1} were assigned to the ν(NH) or $\nu(NH_2)$ stretching vibrations of the piperazinyl moiety. The carboxylate $\nu(C{=}O)_{carb}$ stretching vibration at 1586 cm^{-1} of

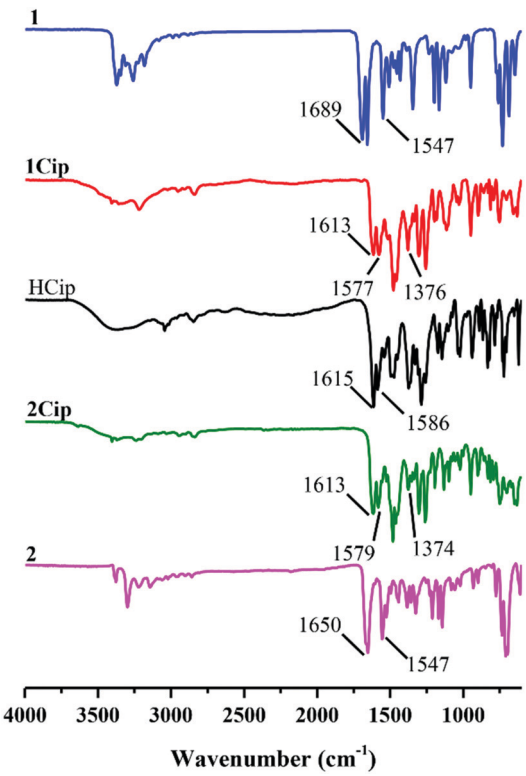

Fig. 2 Overlayered infrared spectra of the starting compounds (**1** and **2**), the mixed-ligand complexes (**1Cip** and **2Cip**) and ciprofloxacin (HCip).

HCip was replaced with two characteristic bands at 1577 and 1376 cm^{-1} for **1Cip** and 1579 and 1374 cm^{-1} for **2Cip**, corresponding to the asymmetric $\nu_{as}(CO_2)_{carb}$ and symmetric $\nu_s(CO_2)_{carb}$ stretching vibrations, respectively. To determine the coordination mode of HCip, the frequency separation ($\Delta\nu = \nu_{as}(CO_2) - \nu_s(CO_2)$) was calculated and found to be in the range of 201–205 cm^{-1} (Table 1), thus suggesting that the carboxylate group of HCip coordinates with the metal center *via* a unidentate bonding nature.[38] In addition, the pyridone $\nu(C{=}O)_{py}$ asymmetric stretching vibration of HCip was slightly shifted from 1615 cm^{-1} to 1613 cm^{-1} upon complexation. Such results indicate that the carboxylate and pyridone oxygen atoms of Cip^{-} coordinate with the copper(II) center.

 This journal is © The Royal Society of Chemistry and the Centre National de la Recherche Scientifique 2022

Table 1 Selected infrared bands and electronic absorption data of ciprofloxacin (HCip), the starting compounds (**1** and **2**), the mixed-ligand complexes (**1Cip** and **2Cip**), and the related compounds

Compound	Wavenumber (cm^{-1})					Electronic absorption, λ_{max} (nm, cm^{-1})	
	$\nu(C{=}O)_{py}$	$\nu(C{=}O)$	$\nu_{as}(CO_2)$	$\nu_s(CO_2)$	Δ^a	Solid	Solution[b]
Ciprofloxacin, HCip	1615	1586	—	—	—	—	—
$[CuL^{1m}Cl_2]_2$, **1**	—	—	—	—	—	670, 14 925	697, 14 347
$[CuL^{2m}Cl_2]_2$, **2**	—	—	—	—	—	636, 15 723	658, 15 198
$[CuL^{1m}(Cip)]Cl$, **1Cip**	1613	—	1577	1376	201	562, 17 794	572, 17 483
$[CuL^{1m}(Cip)]Cl$, **2Cip**	1613	—	1579	1374	205	556, 17 986	578, 17 301
$[Cu(cyclops)]ClO_4{\cdot}H_2O$[c]	—	—	—	—	—	520, 19 231	—
$CuL^1X_2{\cdot}nH_2O$[d]	—	—	—	—	—	588–526, 17 000–19 000	—
$[Cu\text{-}Cip_2]$[e]	—	—	—	—	—	—	516, 19 380

[a] $\Delta = \nu_{as}(CO_2) - \nu_s(CO_2)$. [b] Dissolved in MeOH. [c] Ref. 40 (cyclops = 1,1-difluoro-4,5,11,12-tetramethyll-1-bora-3,6,10,13 tetraaza-2,14 dioxocyclotetradeca-3,5,10,12-tetraenate). [d] Ref. 41 (L^1 = *N*,*N*′-bis(benzimidazol-2-ylethyl)-ethane-1,2-diamine, X = Cl, Br or NO_3). [e] Ref. 42.

ESI-MS spectra in the positive mode of the mixed-ligand complexes (**1Cip** and **2Cip**) confirm the formation of the complexes (Fig. 3). The presence of $[CuL^{1m}(Cip)]^+$ species for **1Cip** and $[CuL^{2m}(Cip)\text{-}H]^{2+}$ species for **2Cip** was identified at m/z = 509 and 599, respectively. The peak at m/z = 332 in the mass spectra of both complexes may be assigned to $[HCip + H]^+$ species, which could indicate the presence of ciprofloxacin in the products. These obtained results are consistent with the data from elemental analysis. This led to the proposed formulae of $[CuL^{1m}(Cip)]Cl$ for **1Cip** and $[CuL^{2m}(Cip)]Cl$ for **2Cip**.

To further investigate the binding of Cip^- to the copper center and predict the stereochemistry of the products, the electronic spectrum in the solid state (diffuse reflectance) and in methanol solution (UV-Visible) of the starting compounds (**1** and **2**) and the mixed-ligand complexes (**1Cip** and **2Cip**) were recorded at room temperature, as illustrated in Fig. 4. Their maximum absorptions are given in Table 1.

The blue color of the starting compounds (**1** and **2**) changed to purple for the mixed-ligand complexes (**1Cip** and **2Cip**), thus preliminarily suggesting that the environments around the copper centers of the mixed-ligand complexes differ from the starting compounds. Moreover, in comparison with **1** and **2**,

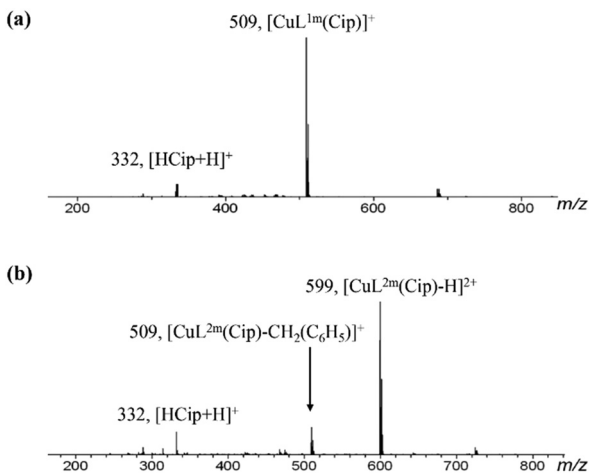

Fig. 3 ESI-MS spectra of (a) **1Cip** and (b) **2Cip** in DMSO : EtOH (1 : 3, v/v) at 125 K.

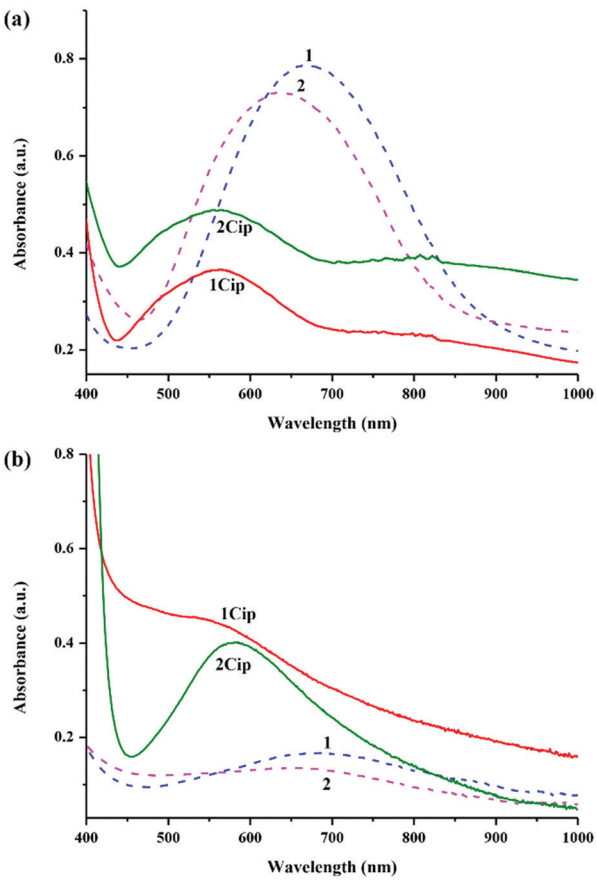

Fig. 4 (a) Diffuse reflectance and (b) UV-Visible spectra of the starting compounds (**1** and **2**) compared with the mixed-ligand complexes (**1Cip** and **2Cip**).

the d–d absorption bands of **1Cip** and **2Cip** shifted to shorter wavelengths and were observed to be in the region of 556–562 nm (17 986–17 794 cm^{-1}) in the solid phase and 572–578 nm (17 483–17 301 cm^{-1}) in the solution phase. This indicates that the ligands interact with the copper center and may adopt a square planar geometry with the CuN_2O_2 chromophore.[39] According to the literature reviews, the copper(II) complexes containing the *N*,*N*-bidentate ligands such

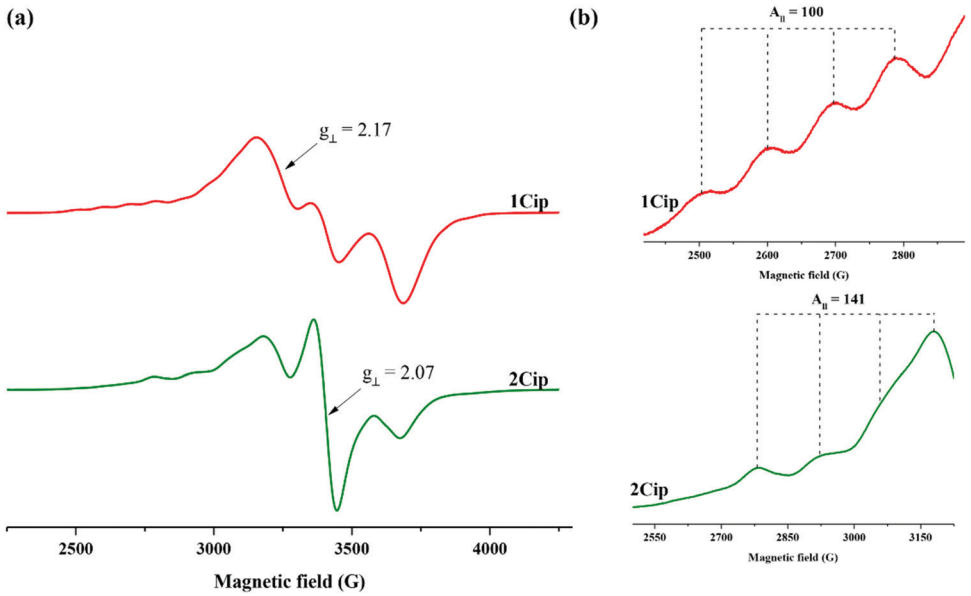

Fig. 5 (a) EPR spectra and (b) hyperfine splitting of **1Cip** and **2Cip**.

as [Cu(cyclops)]$ClO_4 \cdot H_2O$[40] and $[CuL^1X_2] \cdot nH_2O$[41] or ciprofloxacin, [Cu-Cip_2],[42] adopt a square planar geometry with the CuN_4 or CuO_4 chromophores, which show a maximum absorption band similar to our complexes, in the range of 17 000–19 380 cm^{-1} (Table 1).

To further confirm the geometry of the mixed-ligand complexes (**1Cip** and **2Cip**), the EPR spectra in the solid state were recorded at room temperature (Fig. 5). The Spin Hamiltonian parameters are significantly related to the type of donor atoms, and thus, can provide information on the stereochemistry of the complexes. The EPR spectra of **1Cip** and **2Cip** displayed a typical anisotropic spectrum of monomeric copper(II) complexes containing four hyperfine lines in the $g_\parallel$ region due to the interaction of the $S = 1/2$ electron spin with the $I = 3/2$ copper nucleus. In comparison with the g values of their starting compounds and an unpaired electron (2.0023), the $g_\parallel$ values of **1Cip** and **2Cip** were shifted to higher magnetic fields in the range of 2.36–2.67 (Table 2), indicating that the Cip^- possibly interacts with the copper center. Moreover, their $g_\parallel$ values are higher than the $g_\perp$ values ($g_\parallel > g_\perp > 2.0023$), suggesting that the unpaired electron of the copper(II) is located in a $d_{x^2-y^2}$ orbital of an axial square-based geometry.[43,44] To uncover the exchange interactions between the copper centers in polycrystalline complexes, the G values were calculated (Table 2). If $G > 4$, the exchange interaction is negligible, while $G < 4$ indicates a considerable exchange interaction.[43,45] According to these data, the G values > 4 of both **1Cip** and **2Cip** show that there are no exchange interactions between the copper centers in the solid state. In addition, the $g_\parallel/A_\parallel$ values, which can tell us the degree of distortion of the square-planar geometry around the copper atom, of 267 and 167 cm for **1Cip** and **2Cip**, respectively, indicate that **1Cip** has considerable distortion but **2Cip** has only small to moderate distortion.[46,47]

Table 2 Spin Hamiltonian parameters of the starting compounds (**1** and **2**) and the mixed-ligand complexes (**1Cip** and **2Cip**)

Compound	$g_\parallel$	$g_\perp$	G^a	$A_\parallel$ (G)	$g_\parallel/A_\parallel$ (cm)
$[CuL^{1m}Cl_2]_2$, **1**[b]	2.28	2.06	4.81	168	—
$[CuL^{2m}Cl_2]_2$, **2**[b]	2.27	2.06	4.64	158	—
$[CuL^{1m}(Cip)]Cl$, **1Cip**	2.67	2.12	5.67	100	267
$[CuL^{2m}(Cip)]Cl$, **2Cip**	2.36	2.07	5.28	141	167

[a] $G = (g_\parallel - 2.0023)/(g_\perp - 2.0023)$. [b] Ref. 20.

3.2 DFT calculations

To explore the possible geometries of the synthesized **1Cip** and **2Cip** complexes, selected geometries of both complexes have been optimized at the B3LYP/def2-TZVP level of theory in the gas phase. Three different configurations were optimized, including a distorted square planar (A and B) and a distorted square pyramid (C), as shown in Fig. 6.

From all three configurations (A, B and C), the copper atom coordinates through the oxygen atoms of pyridine (O1) and carboxylate (O2) groups of the deprotonated ciprofloxacin (Cip^-) in a bidentate fashion. The bonding between the central copper atom with the guanidine-based ligand and the Cl atom differs in each configuration. For configuration A, the copper atom binds to the N1 and N2 atoms of the guanidine-based ligand, forming a four-fold complex, while the Cl acts as a counter ion. Similarly, in the B form, the copper atom also forms a four-fold-coordinated complex, but it binds with the N1 atom of the guanidine-based ligand and a Cl atom. In contrast, in the C form, while both Cip^- and the guanidine-based ligands bidentately bind to the copper center, the copper atom additionally coordinates with the Cl atom, forming a five-fold-coordinated complex.

In considering the binding energy from eqn (1), 1A and 2A exhibit the lowest binding energies among the three different

 This journal is © The Royal Society of Chemistry and the Centre National de la Recherche Scientifique 2022

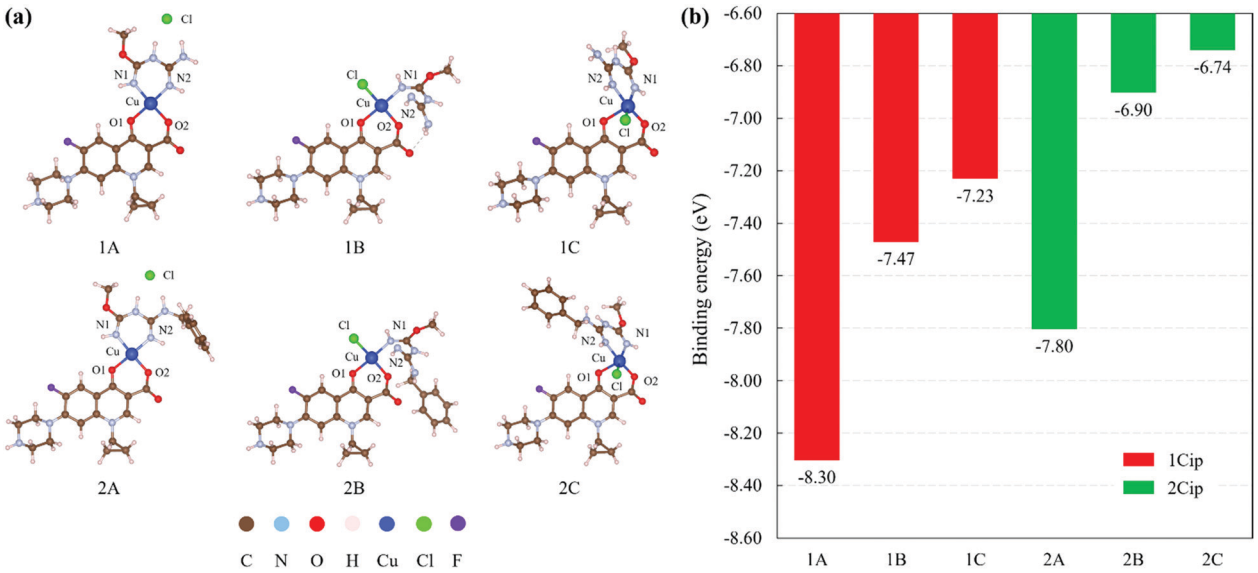

Fig. 6 (a) Optimized geometries of **1Cip** and **2Cip** complexes and (b) their binding energies computed at the B3LYP/def2-TZVP level of theory.

configurations of the analogs for both **1Cip** and **2Cip**. As shown in Fig. 6(b), for the **1Cip** complex, the 1A configuration (−8.30 eV) is significantly more stable than the 1B (−7.47 eV) or 1C (−7.23 eV) configurations. The same trend is also found in the **2Cip** complex, where the 2A configuration (−7.80 eV) is much more stable than the 2B (−6.90 eV) or 2C (−6.74 eV) configurations. The calculated results suggest that the distorted square planar orientation of the A configuration is preferred over the B configuration or the distorted square pyramid (C).

To better understand the origin of such a stable configuration of the distorted square planar (A), we closely examined some important parameters of the optimized geometrical structures, as summarized in Table S2 of the ESI.† The optimized **1Cip** complex is inappreciably different from the **2Cip** complex with the same form. For the distorted square planar geometries (A) of **1Cip** (1A) and **2Cip** (2A), the bond lengths of Cu–O1 and Cu–O2 are in the range of 1.970–1.971 and 1.918–1.919 Å, respectively. The O1–Cu–O2 angles of both compounds range from 93.31° to 93.42°. For the guanidine-based ligand, the Cu–N1 and Cu–N2 bonds are 1.954 and 1.947 Å long, while the N1–Cu–N2 angle is between 88.49° and 88.68°. The geometrical parameters for each configuration show small deviations compared with its analog.

Next, the geometrical parameters of the complexes were further compared in the same system. For the **1Cip** complex, the bond distances between the copper center and the donor atoms are shorter in the A form compared with the B and C forms (Table S2, ESI†), *i.e.*, the Cu–O1 bond of 1.970 Å for 1A is shorter than those of 1.980 and 2.294 Å for 1B and 1C, respectively; the Cu–N1 bond of 1.954 Å for 1A is shorter than those of 2.004 and 2.076 Å for 1B and 1C, respectively. This trend is also found in the **2Cip** complex in which the A form exhibits shorter distances between the copper atom and the donor atoms. Thus, the distorted square planar geometry (A) exhibits stronger metal–ligand interactions than those of B and the distorted square pyramid (C), respectively. Such findings are consistent with the binding energies of the A form, which has the highest stability among the studied forms. This may be due to the strong interactions between copper and the ligands.

3.3 Stability of 1Cip and 2Cip

Since the complexes were tested in a solution for DNA interaction and *in vitro* cytotoxicity, it was necessary to investigate their stability in the presence of Tris-buffer containing 0.3% DMSO at 0–72 h. The stability of the complexes was monitored by using UV-Visible spectroscopy. The kinetic rate constants and half-lives [rate constants (k), half-lives ($t_{1/2}$)] were calculated from $t_{1/2} = \ln(2)/k$ (Fig. S1, ESI†). The results showed that the absorbance spectra of **1Cip** and **2Cip** in Tris-buffer containing 0.3% DMSO do not significantly change over time (0 to 72 h). This behavior indicates that both complexes are stable in this solution. The $t_{1/2}$ values for **1Cip** and **2Cip** were calculated and found to be 495 h and 385 h, respectively. Such a result indicates that these compounds could be stable enough to carry out the DNA binding and cytotoxicity experiments.

3.4 DNA binding studies

Transition metal complexes with diverse organic ligands play a role in inhibiting the growth of cancer cells.[48,49] Thus, understanding the binding ability of the complex with DNA is essential to the development and evaluation of potential medical applications. In principle, metal complexes are known to bind to DNA through covalent and/or non-covalent binding modes. In the covalent binding mode, the metal center can directly bond to the nitrogen atoms of nucleobases on the DNA strand.[50] On the other hand, the non-covalent DNA interactions are divided into three possible modes; (i) intercalation between two adjacent DNA base pairs, (ii) groove binding (major and minor grooves) *via* hydrogen bonds or van der Waals forces, or (iii) electrostatic forces on the sugar-phosphate backbone of the

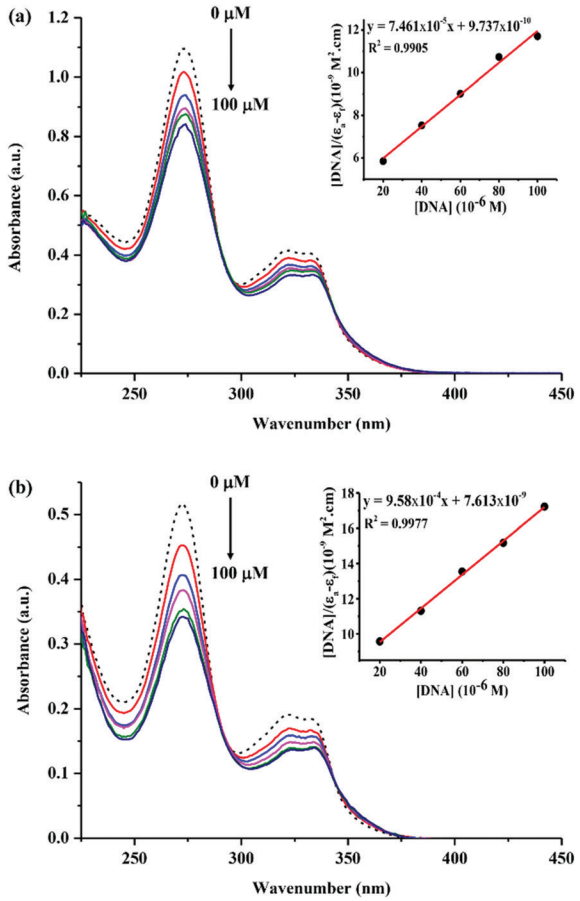

Fig. 7 Absorption titration spectra of (a) **1Cip** and (b) **2Cip** (50 μM) in the absence (---) and presence (—) of CT-DNA (0–100 μM) after incubation at 37 ± 0.1 °C for 24 h. Inset: Plot of [DNA]/($\varepsilon_a - \varepsilon_f$) *vs.* [DNA]. The arrows indicate the intensity change upon increasing concentrations of CT-DNA.

helix.[51] In the present work, the interactions of the complexes with CT-DNA were carefully investigated by electronic absorption titration, viscosity measurement, circular dichroism spectroscopy, and fluorescence titration experiments.

3.4.1 Absorption titration experiments. The changes in intensity observed in the UV-Visible absorption bands of the complexes with different concentrations of CT-DNA make it possible to investigate the DNA binding modes. In principle, small molecules insert into base pairs of DNA through the intercalation mode, showing hypochromism and bathochromism in the absorption intensity, which arises from strong $\pi \rightarrow \pi^*$ stacking interactions of the planar aromatic moieties between the base pairs of DNA.[52,53] In contrast, non-intercalation modes lead to a hyperchromic effect.[54] The absorption spectra of **1Cip** and **2Cip** in the absence and presence of CT-DNA are illustrated in Fig. 7. The intrinsic binding constants (K_b) of the mixed-ligand complexes are summarized in Table 3.

Upon increasing the concentrations of CT-DNA, absorption bands of both **1Cip** and **2Cip** exhibit hypochromism and slight bathochromism (~1 nm), which arise from the π–π* charge transfer transitions of the Cip^- ligand (Fig. 7).[55] In addition, the percentages of hypochromism of both mixed-ligand complexes upon binding to DNA were found to be 23.9% for **1Cip** and 34.0% for **2Cip**, observed at 272–273 nm. These results reveal that the mixed-ligand complexes may interact with CT-DNA through the intercalation mode. The intrinsic binding constants (K_b) of **1Cip** and **2Cip** were calculated by the Wolfe–Shimer eqn (2), and the plots of [DNA]/($\varepsilon_a - \varepsilon_f$) *vs.* [DNA] are depicted in Fig. 7. According to the K_b values in Table 3, **2Cip** exhibits stronger DNA binding potential than **1Cip**. Such a result may be due to the existence of the phenyl ring of the $\mathbf{L^{2m}}$ ligand in **2Cip**, which possibly triggers an additional interaction, *i.e.* intercalation, with DNA. This is in contrast to the starting compounds (**1** and **2**), which showed the opposite situation (hyperchromism effect) to **1Cip** and **2Cip**. The K_b values of **1Cip** and **2Cip** are slightly higher than those of **1** and **2** (Table 3), suggesting that the addition of ciprofloxacin (HCip) as a second ligand may improve the DNA binding capacity of **1Cip** and **2Cip**. However, their K_b values are lower than the classical intercalator, ethidium bromide (EB), since they have less π-conjugated aromatic area, and the aromatic rings of EB are similar to the rings of the bases in DNA, leading to easier π–π stacking interaction,[10] while the K_b value of **2Cip** is higher than those of other previously reported metal complexes containing Cip^- (Table 3). It is probable that the steric structures of $M(Cip)_2(H_2O)_2$,[13] $[Cu(Cip)(A^{1-5})Cl]$[34] and $[Cu(Cip)_2(OH)_2]$[56] make interaction with DNA difficult. To confirm their DNA-binding behaviors, it was necessary to carry out

Table 3 The effect on intensity of the complex-DNA, DNA binding constants (K_b), Stern–Volmer constants (K_{sv}) and apparent binding constants (K_{app})

	Electronic absorption titration		Fluorescence titration			
Compound	Effect on intensity	K_b (M^{-1})	Effect on intensity	K_{sv} (M^{-1})	K_{app} (M^{-1})	Ref.
Ethidium bromide (EB)	Hypochromism	5.35×10^6	Hypochromism	—	1.00×10^7	10 and 33
$[CuL^{1m}Cl_2]_2$, **1**	Hyperchromism	5.63×10^4	—	—	—	10
$[CuL^{2m}Cl_2]_2$, **2**	Hyperchromism	1.07×10^5	—	—	—	10
$[CuL^{1m}(Cip)]Cl$, **1Cip**	Hypochromism	7.66×10^4	Hypochromism	1.36×10^4	1.32×10^5	This work
$[CuL^{2m}(Cip)]Cl$, **2Cip**	Hypochromism	1.26×10^5	Hypochromism	3.59×10^5	3.75×10^5	This work
$M(Cip)_2(H_2O)_2$[a]	Hyperchromism	1.57×10^4–8.71×10^4	Hypochromism	4.47×10^5–7.13×10^5	—	13
$[Cu(Cip)(A^{1-5})Cl]$[b]	Hypochromism	1.27×10^4–4.73×10^4	—	—	—	34
$[Cu(Cip)_2(OH)_2]$	Hypochromism	1.63×10^3	Hypochromism	1.20×10^4	—	56

[a] M = Mn, Co and Ni. [b] A^{1-5} = *1*, 4′-(4-chloro phenyl)-2,2′:6′,2″-terpyridine; *2*, 4′-(3-chloro phenyl)-2,2′:6′,2″-terpyridine; *3*, 4′-(4-bromo phenyl)-2,2′:6′,2″-terpyridine; *4*, 4′-(3-bromo phenyl)-2,2′:6′,2″-terpyridine and *5*, 4′-(4-fluoro phenyl)-2,2′:6′,2″-terpyridine.

 This journal is © The Royal Society of Chemistry and the Centre National de la Recherche Scientifique 2022

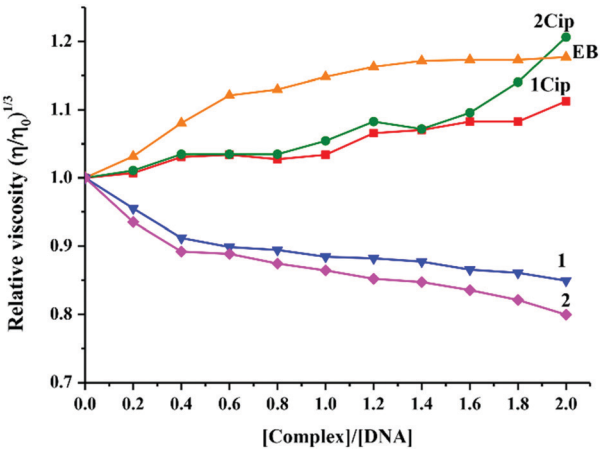

Fig. 8 The relative viscosity of DNA solution (50 μM) upon the addition of ethidium bromide (EB) and the complexes (0–100 μM) in Tris-buffer containing 0.3% DMSO at 37.0 ± 0.1 °C.

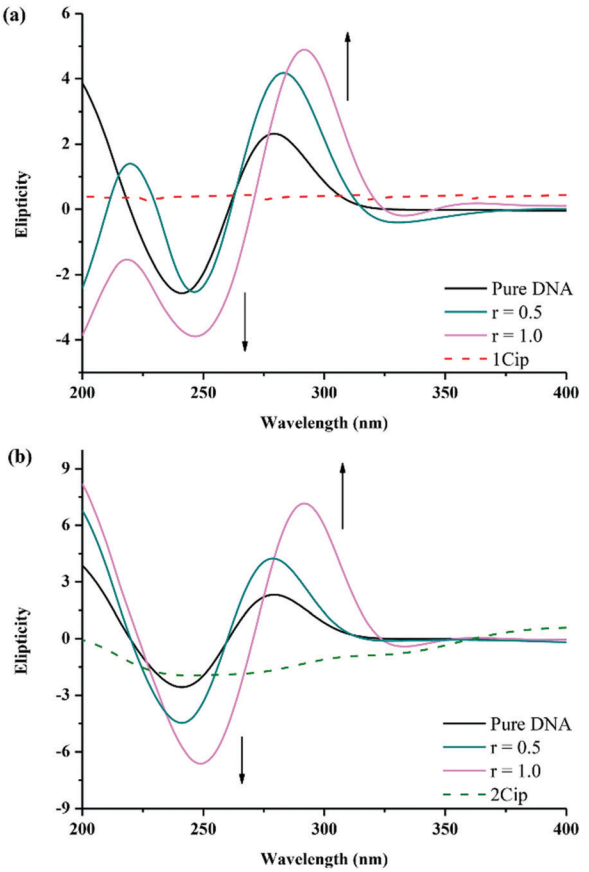

Fig. 9 CD spectra of CT-DNA in the absence and presence of (a) **1Cip** and (b) **2Cip** in Tris-buffer containing 0.3% DMSO, with incubation at 37.0 ± 0.1 °C for 24 h.

further experiments, including viscosity, circular dichroism, and fluorescence emission titration tests.

3.4.2 Viscosity measurements. The binding modes of the complexes were further investigated by viscosity measurements. In the intercalation mode, the viscosity of DNA is increased because the molecule inserts between the base pairs of DNA, leading to the elongation of the double-helix.[57] On the other hand, a dramatic reduction in viscosity is observed in the case of the non-intercalation mode. Meanwhile, a few changes were observed in the DNA viscosity when the molecule interacted with DNA through electrostatic interaction or groove binding.[58] The effects of the complexes on the relative viscosity of CT-DNA are shown in Fig. 8.

Both **1Cip** and **2Cip** exhibit similar effects to EB, thus suggesting that they possibly bind to DNA *via* the intercalation mode. However, they have the opposite results to the starting compounds (**1** and **2**), which decrease the viscosity of DNA. Such a result indicates that the presence of Cip^- may trigger different DNA binding modes and/or an additional site for binding to DNA strands. The results from viscosity measurements are in good agreement with electronic absorption titration.

3.4.3 Circular dichroism spectroscopy (CD). This technique is another tool that is useful in assessing possible structure changes in CT-DNA induced by metal complexes. Normally, CD spectra of CT-DNA show a positive band at 275 nm, and a negative band at 245 nm, corresponding to $\pi \rightarrow \pi^*$ base stacking and the right-handed helicity characteristic of B-DNA, respectively.[59] In intercalation mode, the intensities of both bands are increased because the planar aromatic moiety in metal complexes can stabilize the double helical conformation of DNA. In contrast, the interactions of DNA and complexes through electrostatic forces or groove binding cause few or no perturbations of the base stacking and helicity bands.[60] The CD spectra of CT-DNA in the presence of **1Cip** and **2Cip** (the [Complex]/[DNA] ratio (r) = 0.0, 0.5 and 1.0) are illustrated in Fig. 9.

Upon increasing the concentrations of **1Cip** and **2Cip** in DNA solution, the intensity of both the positive and negative bands was enhanced with the increased [Complex]/[DNA] ratios. Such a result suggests that **1Cip** and **2Cip** may interact with DNA *via* intercalation mode, which differs from their starting compounds.[10] At r = 1.0, the intensity of both the positive and negative bands significantly increased with a large blue-shift (10–12 nm). The large modification in intensity of the CD spectra may indicate some changes in the secondary structure of CT-DNA induced by **1Cip** and **2Cip**.[61] This may be due to the presence of the Cip^- ligand, which may enhance the DNA-binding potential due to the strong $\pi \rightarrow \pi$ interaction between the ligand and the base pairs of DNA.

3.4.4 The fluorescence titration experiments. A competitive binding analysis using fluorescence spectroscopy was carried out to provide further evidence for the binding modes between the complexes and CT-DNA. Ethidium bromide (EB), which emits fluorescence at 610 nm when bound to DNA through its planar aromatic ring between the base pairs of DNA (EB–DNA), was employed as a fluorescence intercalator.[62] The fluorescence emission band of EB–DNA would be quenched if the complexes were able to intercalate between the base pairs of DNA and displace the bound EB. The emission spectra of the EB–DNA in the absence and presence of **1Cip** and **2Cip** are shown in Fig. 10. The Stern–Volmer quenching

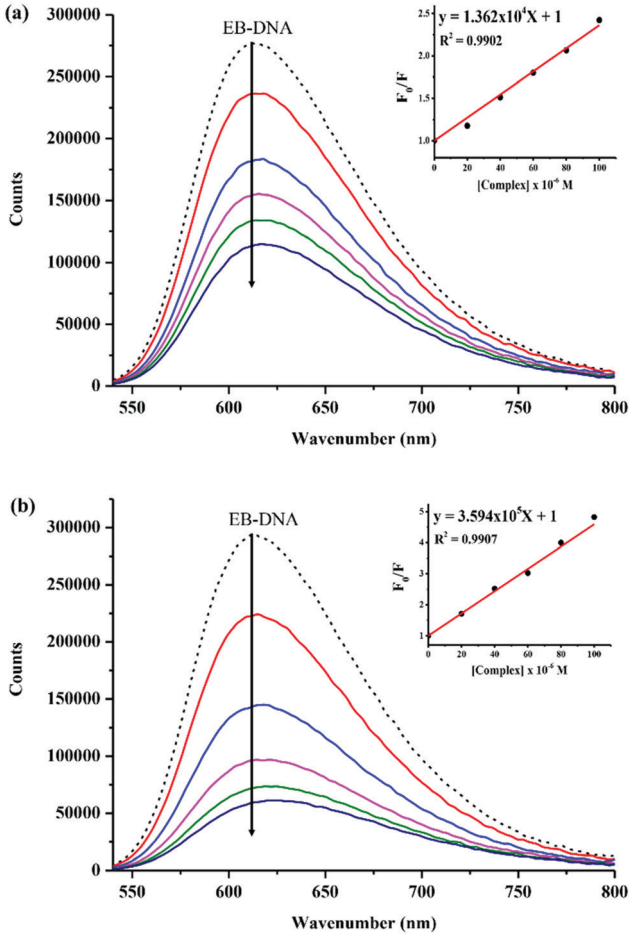

Fig. 10 Emission spectra of EB–DNA (50 μM) in the absence and presence of (a) **1Cip** and (b) **2Cip** (0–100 μM). Inset: Plot of (F_0/F) *vs.* [Complex]. The arrows indicate the emission intensity changes upon increasing concentrations of the complexes.

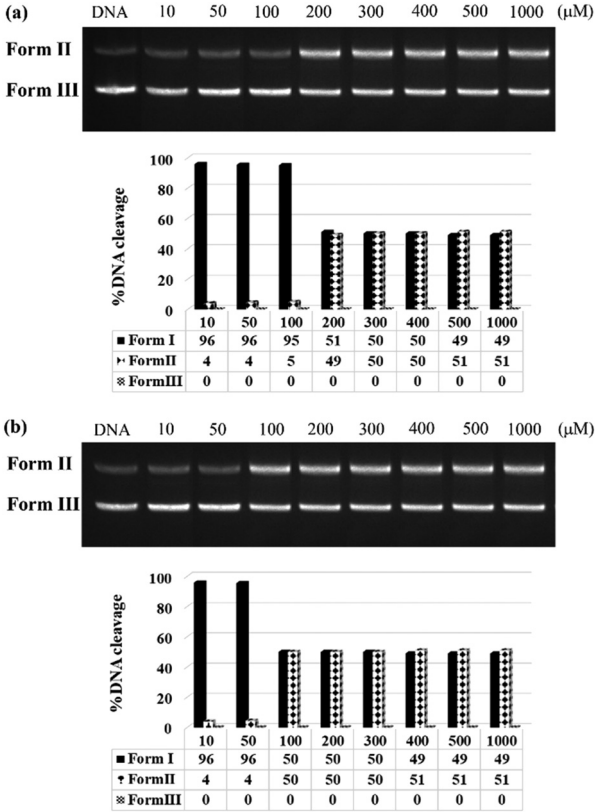

	10	50	100	200	300	400	500	1000
Form I	96	96	95	51	50	50	49	49
FormII	4	4	5	49	50	50	51	51
FormIII	0	0	0	0	0	0	0	0

	10	50	100	200	300	400	500	1000
Form I	96	96	50	50	50	49	49	49
FormII	4	4	50	50	50	51	51	51
FormIII	0	0	0	0	0	0	0	0

Fig. 11 Cleavage of plasmid pBR322 DNA (0.2 μg) by the different concentrations (0–1000 μM) of (a) **1Cip** and (b) **2Cip** in Tris-buffer containing 0.3% DMSO at 37.0 ± 0.1 °C for 4 h.

constants (K_{sv}) and apparent binding constants (K_{app}) are listed in Table 3.

The emission intensity of the EB–DNA with increasing concentrations of the mixed-ligand complexes exhibited a significant hypochromic effect at 59% for **1Cip** and 79% for **2Cip.** These results indicate that the complexes possibly displace EB and strongly interact with DNA *via* the intercalative binding mode. The K_{sv} and K_{app} values were calculated and found to be in the order of EB > **2Cip** > **1Cip.**[33] The DNA binding abilities of the complexes are in good agreement with their K_b values (Table 3) and when the results were compared to data collected from a literature review (Table 3), and it was found that the K_{sv} value of **2Cip** was greater than that of $[Cu(Cip)_2(OH)_2]$,[56] but close to that of the $M(Cip)_2(H_2O)_2$.[13] Such results indicate that **2Cip** containing an aromatic ring on the L^{2m} ligand, and Cip^- can improve DNA binding ability, corresponding with the results from absorption titration, viscosity, and CD experiments.

3.5 DNA cleavage studies

The DNA cleavage efficiency of **1Cip** and **2Cip** was determined by a gel electrophoresis experiment. In general, plasmid pBR322 DNA is divided into three forms: (i) supercoiled (Form I), (ii) open circular (Form II), or (iii) linear (Form III). The normal form of plasmid pBR322 DNA is Form I, which has been observed to produce the fastest migration on gel. If one strand of DNA is cleaved, the supercoiled form (Form I) will relax into the open circular form (Form II), which is the slowest moving on gel. On the other hand, the linear form (Form III) is created by cutting both DNA stands, and migrates between Form I and Form II.

An electrophoretic diagram of DNA in the presence of **1Cip** and **2Cip** (Fig. 11) reveals that only DNA Form II increased in quantity due to single-strand scission of DNA Form I initiated from 200 μM for **1Cip** (Fig. 11(a)), and 100 μM for **2Cip** (Fig. 11(b)). This suggests that the DNA cleavage activity of **2Cip** is superior to that of **1Cip**. Moreover, both **1Cip** and **2Cip** exhibited much greater DNA cleaving ability than did the starting compounds (**1** and **2**).[10] This may result from the presence of ciprofloxacin as a secondary ligand, which is consistent with their DNA binding properties.

To enhance the DNA cleaving ability of **1Cip** and **2Cip**, H_2O_2 (10 μM) as an oxidant agent was added in the same conditions (Fig. 12). It was found that DNA Form I can be cut to create Form II and Form III. Meanwhile, the H_2O_2 itself does not cause any DNA degradation (Fig. 12). At 80 μM and 100 μM, **1Cip** completely cleaved Form I into Forms II and III

 This journal is © The Royal Society of Chemistry and the Centre National de la Recherche Scientifique 2022

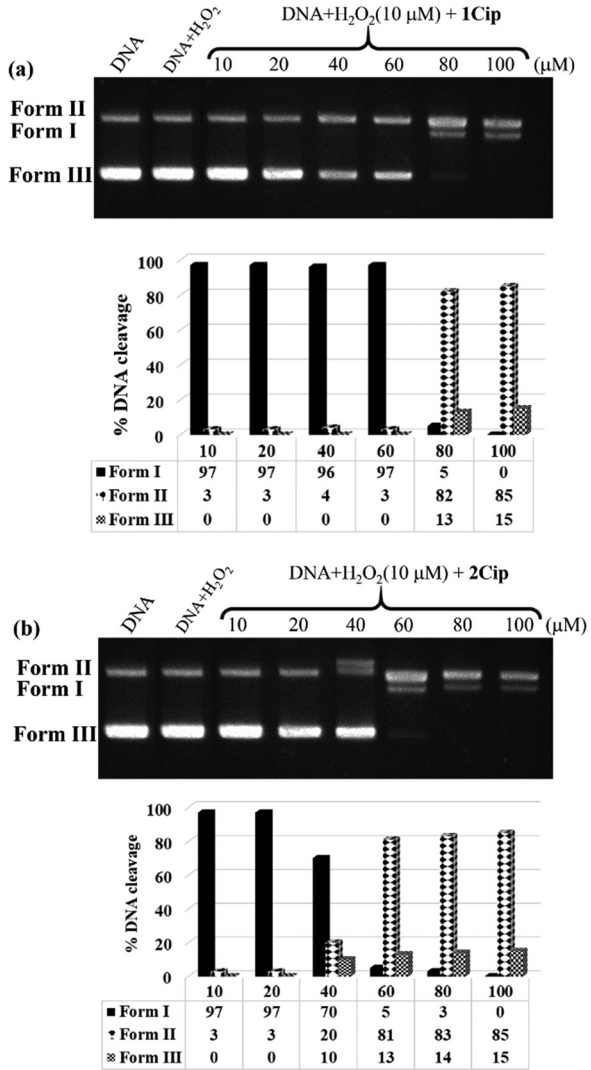

Fig. 12 Cleavage of plasmid pBR322 DNA (0.2 μg) by the different concentrations (0–100 μM) of (a) **1Cip** and (b) **2Cip** in the presence of H_2O_2 (10 μM) in Tris-buffer containing 0.3% DMSO at 37.0 ± 0.1 °C for 1 h and the percentage of DNA cleavage in each form when treated by the complexes.

(Fig. 12(a)). Meanwhile for **2Cip**, the band intensity of Form II considerably increased at 40 μM, and from 60 μM upward, DNA Form I was completely cleaved into Forms II and III (Fig. 12(b)). Such results show that the efficiency in cleaving the DNA of **2Cip** in the presence of H_2O_2 is significantly greater than that of **1Cip**. The DNA cleavage mechanism of the complexes in the presence of H_2O_2 under an aerobic environment was further investigated, and is proposed to be an oxidative pathway. This mechanism pathway involves the formation of reactive oxygen species (ROS) such as hydroxyl radicals ($OH^{\bullet}$) *via* the Fenton mechanism (eqn (7) and (8)), causing DNA damage.[63]

$$Cu(II) + O_2 \rightarrow Cu(I) + O_2^{\bullet -} \quad (7)$$

$$Cu(I) + H_2O_2 \rightarrow Cu(II) + OH^- + {}^{\bullet}OH \quad (8)$$

3.6 Cytotoxicity and mechanisms of cell death

3.6.1 Anticancer activity. The promising results from the DNA binding and cleavage studies prompted us to try to determine, using the MTT assay, the antiproliferative activities of **1Cip** and **2Cip** against human cervical cancer (HeLa), human breast cancer (MCF-7), and normal cells (Vero). The anticancer drug cisplatin was used as a positive control. The complexes were tested against all three cell lines in the same condition range, from 0 to 100 μg mL^{-1}. The IC_{50} values for the complexes are listed in Table 4.

Complexes **1Cip** and **2Cip** showed similar results for growth inhibition over time. After 24 h, both complexes were inactive towards all cells. However, after 48 h, **2Cip**, unlike **1Cip**, displayed a cytotoxic effect against HeLa and MCF-7 cells. Meanwhile, after 72 h, both **1Cip** and **2Cip** were active against HeLa and MCF-7 cells (Table 4). Such a results show that **2Cip** is more active and slightly more efficient than **1Cip** toward both types of cancer cells. In comparison to the starting compounds (**1** and **2**) and the free ligand, **1Cip** and **2Cip** were found to have lower IC_{50} values than those compounds, suggesting that they have greater cytotoxicity against cancer cells. The most satisfactory result is that both **1Cip** and **2Cip** did not affect the normal cells (Vero) at all. On the other hand, cisplatin exhibited high cytotoxicity toward HeLa, MCF-7, and Vero cells, which highlights that the complexes containing ciprofloxacin can enhance cytotoxic efficiency specific to cancer cells, and inactive to normal cells.

3.6.2 Apoptosis assay. To further understand the cytotoxicity phenomenon, cell distribution with apoptotic/necrotic features caused by **1Cip** and **2Cip** was investigated by using

Table 4 IC_{50} values for **1Cip**, **2Cip** and the related compounds against HeLa, MCF-7 and Vero cells. All data are the mean and standard errors obtained from three independent experiments

	IC_{50} ± SD (μg mL^{-1})								
	HeLa			MCF-7			Vero		
Compound	24 h	48 h	72 h	24 h	48 h	72 h	24 h	48 h	72 h
HCip	Inactive	Inactive	Inactive	Inactive	Inactive	Inactive	Inactive	45.48 ± 0.53	43.35 ± 0.45
$[CuL^{1m}Cl_2]_2$, **1**	Inactive	Inactive	Inactive	Inactive	47.46 ± 1.23	45.17 ± 0.30	41.82 ± 0.15	33.58 ± 0.65	15.23 ± 0.87
$[CuL^{2m}Cl_2]_2$, **2**	Inactive	29.65 ± 0.59	27.99 ± 0.38	Inactive	46.74 ± 1.20	45.5 ± 0.23	37.99 ± 0.25	30.70 ± 0.27	13.30 ± 0.67
$[CuL^{1m}(Cip)]Cl$, **1Cip**	Inactive	Inactive	30.57 ± 0.66	Inactive	Inactive	43.25 ± 0.88	Inactive	Inactive	Inactive
$[CuL^{2m}(Cip)]Cl$, **2Cip**	Inactive	28.32 ± 1.22	25.84 ± 1.19	Inactive	43.33 ± 0.88	40.79 ± 1.62	Inactive	Inactive	Inactive
Cisplatin	5.12 ± 0.30	2.99 ± 0.10	2.93 ± 0.04	8.75 ± 1.35	4.12 ± 0.54	3.13 ± 0.26	12.86 ± 0.72	3.71 ± 0.19	1.97 ± 0.24

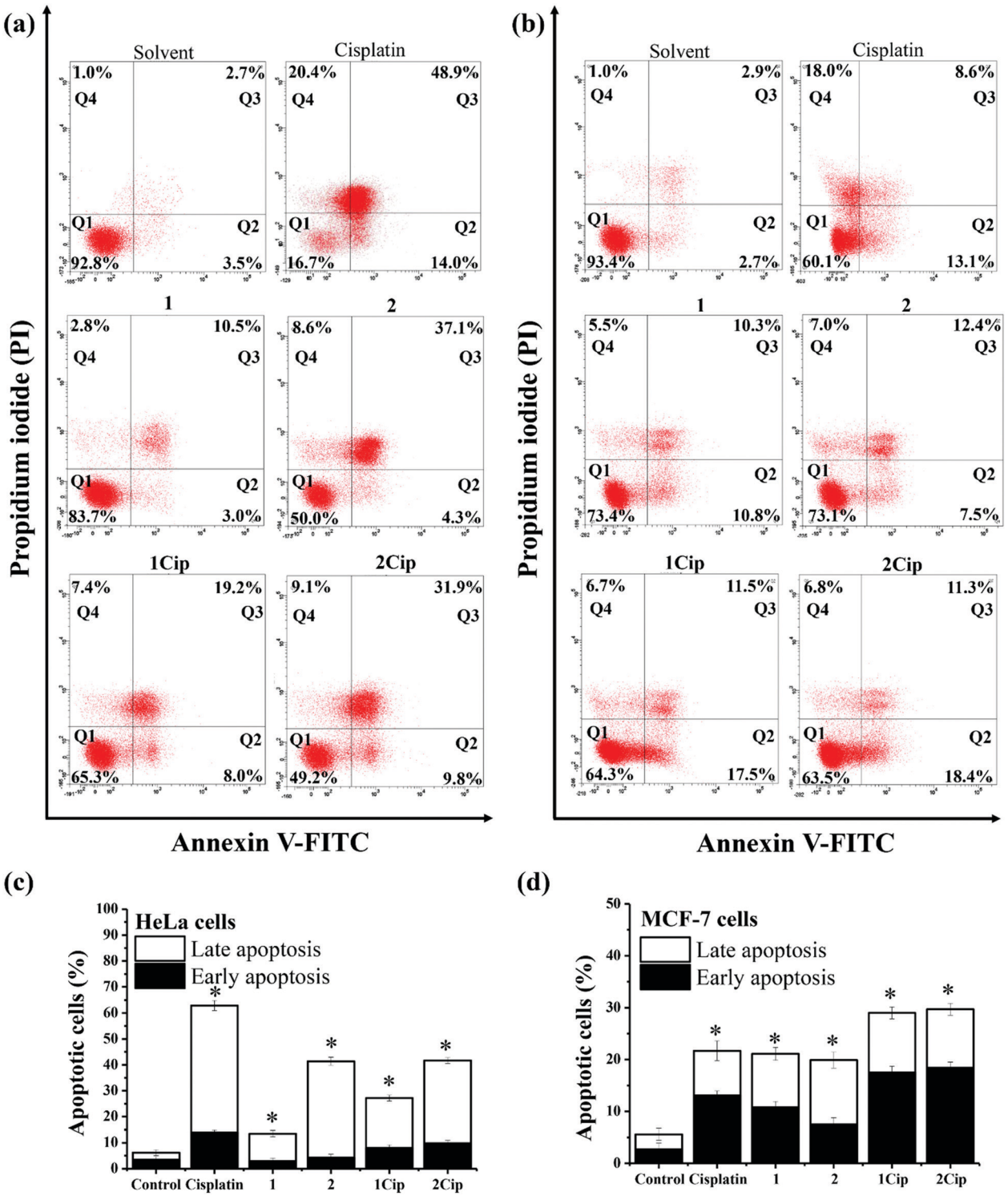

Fig. 13 The representative dot plots of apoptosis induction of (a) HeLa and (b) MCF-7 cells after treatment with **1**, **2**, **1Cip** and **2Cip** (50 μg mL^{-1}) for 48 h with Tris-buffer containing 0.3% DMSO as a solvent control. Percentages of apoptotic cells for (c) HeLa and (d) MCF-7 cell lines. Cisplatin (25 μg mL^{-1}) was used as a positive control. Data represent the mean ± SD of three independent experiments. *$P < 0.01$ significant difference between samples and solvent control.

flow cytometry. In principle, the mechanism of cell death is divided into two pathways: (i) apoptosis and (ii) necrosis. Apoptosis is an important occurrence in cytotoxicity induced by anticancer drugs, and it is associated with morphological characteristics such as chromatin condensation, cell shrinkage, and nuclear fragmentation. On the other hand, necrosis is

 This journal is © The Royal Society of Chemistry and the Centre National de la Recherche Scientifique 2022

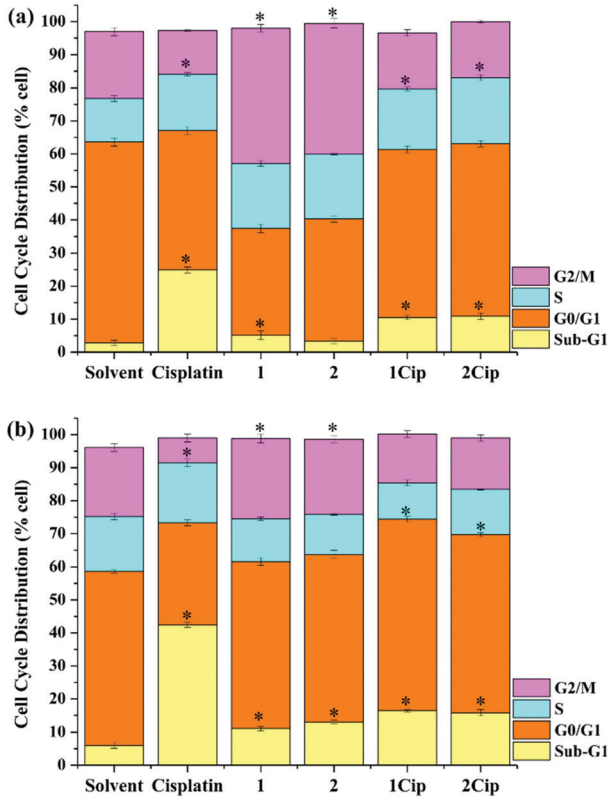

Fig. 14 The percentage of cell cycle distributions of (a) HeLa and (b) MCF-7 cells treated with cisplatin (25 μg mL^{-1}), **1**, **2**, **1Cip** and **2Cip** (50 μg mL^{-1} with Tris-buffer containing 0.3% DMSO) on each cell cycle phase at 48 h. Data represent the mean values of three experiments (±SD). *$P < 0.01$ significant difference between the sample and solvent control.

accidental cell death, which is followed by cell swelling and the inflammation of cells. Apoptosis induction can be detected by double staining with Annexin V-FITC and propidium iodide (PI). Results of this testing are presented in Fig. 13. After 48 h treatment, all complexes (50 μg mL^{-1}) were able to induce cell death of HeLa and MCF-7 through the apoptosis pathway. In HeLa, **2Cip** reduced the number of viable cells, and late apoptosis (Q3) was increased (31.9%) and greater than **1Cip** (19.2%). Meanwhile, there was no difference in the number of apoptotic cells against MCF-7 cells between **1Cip** and **2Cip**. In comparison with their starting compounds (**1** and **2**), both **1Cip** and **2Cip** markedly enhanced the number of early apoptotic cells (Q2) with respect to both HeLa and MCF-7. It is noted that they induced the conversion of cancer cells into necrotic cells (Q4) significantly less than cisplatin. Such a result shows that **1Cip** and **2Cip** containing Cip^- as a secondary ligand could possibly enhance the cytotoxicity toward the two tested cancer cells *via* apoptosis.

3.6.3 cell cycle arrest. The effectiveness of cell cycle arrest in each phase of the cell cycle that is triggered by adding the complexes was determined by flow cytometry. The distribution of cells is divided into three phases, which are G0/G1 phase (2n DNA content), S phase (2n–4n DNA content) and G2/M phase (4n DNA content), where n is the genetic material. In addition, the characteristic of apoptotic cell death is exhibited in sub-G1 due to a small DNA fragmentation (<2n DNA content). The effects of the complexes on each phase of the cell cycle uncovered in this study are shown in Fig. S2 (ESI†). The results of cells in each phase of the cell cycle being in the absence and presence of **1**, **2**, **1Cip** and **2Cip** are listed in Table S3 (ESI†) and Fig. 14.

Treatment of HeLa cells with **1Cip** and **2Cip** increased the cell distribution at the S phase by 18.3% and 19.9%, respectively. This compares to results from the solvent control (13.2%), indicating that **1Cip** and **2Cip** induced cell cycle arrest at the S phase (Fig. 14(a)). On the other hand, MCF-7 cells treated with these complexes exhibited cell cycle arrest at the G0/G1 phase, an increase of 58.0% for **1Cip** and 53.9% for **2Cip**, which is an improved result compared with the solvent control (52.7%) (Fig. 14(b)). Such a result shows a majority of the cell population in different phases of the cell cycle to be in arrest. After treatment with **1Cip** and **2Cip**, the apoptotic cell population was significantly increased in the sub-G1 fractions in both HeLa and MCF-7 cells (Fig. 14). Compared with the starting compounds (**1** and **2**), an increase in cycle arrest at the G2/M phase in both HeLa and MCF-7 cells was observed, while cisplatin inhibited the cell growth at the S phase. According to the obtained results, the presence of Cip^- as an additional ligand probably affects the cell death in different phases.

3.6.4 Antibacterial activity. The antibacterial activity of complexes **1Cip** and **2Cip** containing Cip^- was further tested against *E. coli, Salmonella* and *Campylobacter* by the disc diffusion technique. The inhibition-zone (mm) and the minimum inhibitory concentrations (MICs) are listed in Table 5 and Fig. S3 (ESI†).

Both **1Cip** and **2Cip** demonstrated antibacterial activity against all three tested bacteria; this compares to their starting

Table 5 Inhibition zone and MIC values for HCip, **1**, **2**, **1Cip** and **2Cip**

	Inhibition-zone diameter ± SD (mm)			MIC[a] (μg mL^{-1})		
Compound	*E. coli*	*Salmonella*	*Campylobacter*	*E. coli*	*Salmonella*	*Campylobacter*
Ciprofloxacin, HCip	10.33 ± 1.52	14.33 ± 1.15	Inactive	62.5	1.95	Inactive
$[CuL^{1m}Cl_2]_2$, **1**	Inactive	Inactive	Inactive	Inactive	Inactive	Inactive
$[CuL^{2m}Cl_2]_2$, **2**	Inactive	Inactive	Inactive	Inactive	Inactive	Inactive
$[CuL^{1m}(Cip)]Cl$, **1Cip**	15.00 ± 0.58	20.00 ± 0.00	11.66 ± 1.53	62.5	1.95	250
$[CuL^{2m}(Cip)]Cl$, **2Cip**	12.66 ± 0.55	30.00 ± 0.00	10.00 ± 2.00	31.2	1.95	125
0.3% DMSO/Tris-buffer	Inactive	Inactive	Inactive	Inactive	Inactive	Inactive

[a] MIC means the lowest concentration of the complexes which can prevent the visible growth of bacteria.

complexes (**1** and **2**), which did not demonstrate inhibitory activity (Table 5). Complex **2Cip** exhibited the greatest cytotoxicity, resulting in lower MIC values than **1Cip**. Having considered the results of the antibacterial drug HCip alone, both **1Cip** and **2Cip** displayed good antibacterial activity against all three bacteria, while HCip was inactive toward *Campylobacter*. Such results confirm that the existence of Cip^{-} in the copper(II) complexes possibly enhances the antibacterial activity. Hence, the two mixed-ligand complexes in this present work have promising potential for development as antibacterial agents.

4. Conclusion

In summary, the present report describes two newly synthesized complexes of guanidine derivatives and ciprofloxacin (**1Cip** and **2Cip**) with interesting DNA interaction properties, and biological activities against human cancer cells, and human food poisoning bacteria. All analytical data, together with the DFT calculations, have revealed that both complexes possibly adopt a distorted square planar geometry. These ciprofloxacin-containing compounds have been found to have greater efficiency in DNA-binding and cleavage abilities than their starting compounds (**1** and **2**). Both **1Cip** and **2Cip** exhibited strong binding to CT-DNA by an intercalative mode, with relatively high binding constants. Complex **2Cip** seems to have higher DNA-interacting potential than **1Cip**. The evaluation of the anticancer activity of the complexes by the IC_{50} values found that the ciprofloxacin containing complexes showed better activity than **1**, **2** and free HCip against HeLa and MCF-7. Apparently, they are inactive toward normal cell lines (Vero cells) under the studied conditions. Mechanisms of cell death were further investigated, and it was found that both **1Cip** and **2Cip** induce apoptosis against cancer cells at the S phase for HeLa and the G0/G1 phase for MCF-7, while cisplatin inhibited cell growth at the S phase. Furthermore, antibacterial activity of the complexes was observed against all three tested bacteria, although **1Cip** and **2Cip** showed the best antibacterial activity against *Salmonella*. From all obtained results, the reported complexes are suitable candidates for the next generation of anticancer and/or antibacterial drugs.

Author contributions

P. N. and A. M. performed the experiments, analyzed the data, and prepared the manuscript. T. S. provided normal and cancer cell lines. C. S. and P. C. performed the antibacterial experiment. A. W. and S. S. performed the computational calculations. U. C. conceived the idea, prepared the manuscript, and supervised the work.

Conflicts of interest

We have no conflict of interest to disclose.

Acknowledgements

This work is supported by the Royal Golden Jubilee PhD Program (RGJ-PhD) (Grant No. PHD/0113/2559), the Center of Excellence for Innovation in Chemistry (PERCH-CIC), Office of the Higher Education, Commission, Ministry of Education, Thailand. DFT calculations are supported by NSTDA Supercomputer Center (ThaiSC) for computational resources and Suranaree University of Technology and Thailand Science Research and Innovation (TSRI).

References

1 B. Rosenberg, L. Vancamp and T. Krigas, *Nature*, 1965, **205**, 698–699.
2 U. Ndagi, N. Mhlongo and M. E. Soliman, *Drug Des., Dev. Ther.*, 2017, **11**, 599–616.
3 L. Kou, S. Wei and P. Kou, *Front. Chem.*, 2021, **9**, 733463.
4 Y. Li, B. Liu, H. Shi, Y. Wang, Q. Sun and Q. Zhang, *Dalton Trans.*, 2021, **50**, 14498–14512.
5 L. J. Harvey, K. Ashton, L. Hooper, A. Casgrain and S. J. Fairweather-Tait, *Am. J. Clin. Nutr.*, 2009, **89**, 2009–2024.
6 S. Rajalakshmi, A. Fathima, J. R. Rao and B. U. Nair, *RSC Adv.*, 2014, **4**, 32004–32012.
7 K. Gałczyńska, K. Ciepluch, Ł. Madej, K. Kurdziel, B. Maciejewska, Z. Drulis-Kawa, A. Węgierek-Ciuk, A. Lankoff and M. Arabski, *Sci. Rep.*, 2019, **9**, 9777.
8 A. Hussain, M. F. AlAjmi, M. T. Rehman, S. Amir, F. M. Husain, A. Alsalme, M. A. Siddiqui, A. A. AlKhedhairy and R. A. Khan, *Sci. Rep.*, 2019, **9**, 5237.
9 K. L. McGuire, P. Smit, D. H. Ess, J. T. Hill, R. G. Harrison and D. D. Busath, *Biophys. J.*, 2021, **120**, 168–177.
10 A. Meenongwa, R. F. Brissos, C. Soikum, P. Chaveerach, P. Gamez, Y. Trongpanich and U. Chaveerach, *New J. Chem.*, 2015, **39**, 664–675.
11 D. E. King, R. Malone and S. H. Lilley, *Am. Fam. Physician*, 2000, **61**, 2741–2748.
12 J. Hernández-Gil, L. Perelló, R. Ortiz, G. Alzuet, M. González-Álvarez and M. Liu-González, *Polyhedron*, 2009, **28**, 138–144.
13 G. Psomas, *J. Inorg. Biochem.*, 2008, **102**, 1798–1811.
14 G. J. Kharadi, *Spectrochim. Acta, Part A*, 2011, **79**, 898–903.
15 J. R. Anacona and C. Toledo, *Transition Met. Chem.*, 2001, **26**, 228–231.
16 M. P. López-Gresa, R. Ortiz, L. Perelló, J. Latorre, M. Liu-González, S. García-Granda, M. Pérez-Priede and E. Cantón, *J. Inorg. Biochem.*, 2002, **92**, 65–74.
17 M. N. Patel, C. R. Patel and H. N. Joshi, *Inorg. Chem. Commun.*, 2013, **27**, 51–55.
18 L. H. Abdel-Rahman, R. M. El-Khatib, L. A. E. Nassr, A. M. Abu-Dief, M. Ismael and A. A. Seleem, *Spectrochim. Acta, Part A*, 2014, **117**, 366–378.
19 G. Klopman, S. Wang, M. R. Jacobs, S. Bajaksouzian, K. Edmonds and J. J. Ellner, *Antimicrob. Agents Chemother.*, 1993, **37**, 1799–1806.
20 A. Meenongwa, U. Chaveerach and K. Siriwong, *Inorg. Chim. Acta*, 2011, **366**, 357–365.

 This journal is © The Royal Society of Chemistry and the Centre National de la Recherche Scientifique 2022

21 S. G. Balasubramani, G. P. Chen, S. Coriani, M. Diedenhofen, M. S. Frank, Y. J. Franzke, F. Furche, R. Grotjahn, M. E. Harding, C. Hättig, A. Hellweg, B. Helmich-Paris, C. Holzer, U. Huniar, M. Kaupp, A. M. Khah, S. K. Khani, T. Müller, F. Mack, B. D. Nguyen, S. M. Parker, E. Perlt, D. Rappoport, K. Reiter, S. Roy, M. Rückert, G. Schmitz, M. Sierka, E. Tapavicza, D. P. Tew, C. V. Wüllen, V. K. Voora, F. Weigend, A. Wodyński and J. M. Yu, *Chem. Phys.*, 2020, **152**, 184107.

22 R. Ahlrichs, M. Bär, M. Häser, H. Horn and C. Kölmel, *Chem. Phys. Lett.*, 1989, **162**, 165–169.

23 A. D. Becke, *Chem. Phys.*, 1993, **98**, 1372–1377.

24 C. Lee, W. Yang and R. G. Parr, *Phys. Rev. B: Condens. Matter Mater. Phys.*, 1988, **37**, 785–789.

25 F. Weigend and R. Ahlrichs, *Phys. Chem. Chem. Phys.*, 2005, **7**, 3297–3305.

26 K. Momma and F. Izumi, *J. Appl. Crystallogr.*, 2011, **44**, 1272–1276.

27 P. Štarha, J. Hošek, Z. Trávníček and Z. Dvořák, *Appl. Organomet. Chem.*, 2020, **34**, e5785.

28 M. E. Reichmann, S. A. Rice, C. A. Thomas and P. Doty, *J. Am. Chem. Soc.*, 1954, **76**, 3047–3053.

29 J. Marmur, *J. Mol. Biol.*, 1961, **3**, 208–218.

30 A. Wolfe, G. H. Shimer and T. Meehan, *Biochemistry*, 1987, **26**, 6392–6396.

31 G. Cohen and H. Eisenberg, *Biopolymers*, 1969, **8**, 45–55.

32 J. R. Lakowicz and G. Weber, *Biochemistry*, 1973, **12**, 4161–4170.

33 M. Lee, A. L. Rhodes, M. D. Wyatt, S. Forrow and J. A. Hartley, *Biochemistry*, 1993, **32**, 4237–4245.

34 M. Patel, P. Dosi and B. Bhatt, *Polyhedron*, 2010, **29**, 3238–3245.

35 E. Chacon, D. Acosta and J. J. Lemasters, in *In vitro methods in pharmaceutical research*, ed. J. V. Castell and M. J. Gómez-Lechón, Academic Press, San Diego, 1997, pp. 209–223.

36 C. H. Collins and P. M. Lyne, *Microbiological methods*, University Park Press, Baltimore, 1970.

37 E. J. L. Lana, F. Carazza and J. A. Takahashi, *J. Agric. Food Chem.*, 2006, **54**, 2053–2056.

38 W. Beck and K. Nakamoto, *Infrared and Raman spectra of inorganic and coordination compounds*, John Wiley & Sons, New York, 1988.

39 B. J. Hathaway, *Dalton Trans.*, 1972, 1196–1199.

40 A. W. Addison, M. Carpenter, L. K. M. Lau and M. Wicholas, *Inorg. Chem.*, 1978, **17**, 1545–1552.

41 T. Pandiyan, M. Palaniandavar, M. Lakshminarayanan and H. Manohar, *J. Chem. Soc., Dalton Trans.*, 1992, **1**, 3377–3384.

42 Z. H. Chohan, C. T. Supuran and A. Scozzafava, *J. Enzyme Inhib. Med. Chem.*, 2005, **20**, 303–307.

43 I. M. Procter, B. J. Hathaway and P. Nicholls, *J. Chem. Soc. A*, 1968, 1678–1684.

44 B. J. Hathaway and D. E. Billing, *Coord. Chem. Rev.*, 1970, **5**, 143–207.

45 M. Shakir, S. P. Varkey and P. S. Hameed, *Polyhedron*, 1994, **13**, 1355–1361.

46 A. W. Addison, *Copper coordination chemistry: Biochemical & inorganic perspectives*, 1983, pp. 109–128.

47 V. V. Pavlishchuk, *Theor. Exp. Chem.*, 1995, **31**, 1–26.

48 S. K. Nandanwar and H. J. Kim, *ChemistrySelect*, 2019, **4**, 1706–1721.

49 M. Frezza, S. Hindo, D. Chen, A. Davenport, S. Schmitt, D. Tomco and Q. P. Dou, *Curr. Pharm. Des.*, 2010, **16**, 1813–1825.

50 A. Eastman, in *Cisplatin: Chemistry and biochemistry of a leading anticancer drug*, ed. B. Lippert, VHCA & Wiley-VCH, Zurich & Germany, 1999, pp. 111–134.

51 G. M. Blackburn, M. J. Gait and D. Loakes, in *Nucleic acid in chemistry and biology*, ed. D. M. Williams, Cambridge, RSC Publishing, 2006, pp. 342–382.

52 L. S. Lerman, *J. Mol. Biol.*, 1961, **3**, 18–30.

53 E. C. Long and J. K. Barton, *Acc. Chem. Res.*, 1990, **23**, 271–273.

54 Q. Li, P. Yang, H. Wang and M. Guo, *J. Inorg. Biochem.*, 1996, **64**, 181–195.

55 X. Qiao, Z. Y. Ma, C. Z. Xie, F. Xue, Y. W. Zhang, J. Y. Xu, Z. Y. Qiang, J. S. Lou, G. J. Chen and S. P. Yan, *J. Inorg. Biochem.*, 2011, **105**, 728–737.

56 H. Farrokhpour, H. Hadadzadeh, F. Darabi, F. Abyar, H. A. Rudbari and T. Ahmadi-Bagheri, *RSC Adv.*, 2014, **4**, 35390–35404.

57 P. V. Scaria and R. H. Shafer, *J. Biol. Chem.*, 1991, **266**, 5417–5423.

58 S. Satyanarayana, J. C. Dabrowiak and J. B. Chaires, *Biochemistry*, 1992, **31**, 9319–9324.

59 V. I. Ivanov, L. E. Minchenkova, A. K. Schyolkina and A. I. Poletayev, *Biopolymers*, 1973, **12**, 89–110.

60 B. Nordén and F. Tjerneld, *Biopolymers*, 1982, **21**, 1713–1734.

61 X. B. Fu, D. D. Liu, Y. Lin, W. Hu, Z. W. Mao and X. Y. Le, *Dalton Trans.*, 2014, **43**, 8721–8737.

62 B. C. Baguley and M. Le Bret, *Biochemistry*, 1984, **23**, 937–943.

63 C. H. Chen and D. S. Sigman, *Proc. Natl. Acad. Sci. U. S. A.*, 1986, **83**, 7147–7151.